Calculation of Unsteady Subsonic Flow about Harmonically Oscillating Wing/Body Configurations

R. Roos,* B. Bennekers,† and R.J. Zwaan‡
National Aerospace Laboratory NLR, Amsterdam, The Netherlands

A description is given of a panel method for the calculation of the aerodynamic loading on harmonically oscillating wing/body configurations in subsonic flow. Neglecting their thickness, the loading on the lifting surfaces is assumed to be generated by a distribution of unsteady lifting lines. The loads on the body are represented by an unsteady source panel distribution. A way is indicated to introduce the effect of the steady flow into the unsteady calculations. The method provides local and total coefficients as well as detailed pressure distributions on both the lifting surfaces and the bodies. The applicability of the method is shown in a comparison of calculated and experimental pressure and load distributions on a wing/tip tank/pylon store configuration.

Nomenclature

A^{ij} = influence coefficient
a = velocity of sound
c = local chord
$\bar{c}$ = mean chord
C_p = pressure coefficient
C_y = local side load coefficient; C_y = side load $/ q_\infty \ell_{ref}$
C_z = local normal load coefficient; C_z = normal load $/ q_\infty \ell_{ref}$
K = kernel function
k = reduced frequency
k_n = wave number
ℓ_{ref} = reference length; wing $\ell_{ref} = c$, body ℓ_{ref} = max. diam
ℓ, m, n = components of the normal vector n
M = Mach number
N = number of panels
n = normal vector
q = velocity vector
r_c = distance between collocation point i and the centroid of panel j
r_e = displacement vector
S = surface of wing or body
t = time
t = longest panel diagonal
U, V, W = components of the velocity vector
x, y, z = right-hand Cartesian coordinate system
x_e, y_e, z_e = components of the displacement vector
ΔC_p = pressure jump between lower and upper wing surface
β = $(1-M^2)^{1/2}$
γ = specific heat ratio
δ = angular coordinate on the body, deg
ξ, η, ζ = right-hand Cartesian coordinate system
σ = source strength
φ = perturbation velocity potential
ω = oscillation frequency

Superscripts

B = referring to the body
D = referring to the lifting surface
$*$ = referring to a time-independent quantity

Subscripts

B = referring to the body
D = referring to the lifting surface
n = referring to the steady ($n=0$) and unsteady ($n=1$) flowfield
0 = referring to the steady reference position
1 = referring to the unsteady flowfield
∞ = referring to the freestream condition

Introduction

PRESENT day military aircraft are often equipped with large wing-mounted stores. For the investigation of the aeroelastic characteristics of such aircraft (flutter, gust response, and maneuvering loads), it is necessary to have reliable estimates of the unsteady aerodynamic loading introduced by such stores, both on themselves and on the wing.

Several years ago, the NLR, recognizing this problem, started a research program to investigate the airloads on oscillating wing/body configurations. The first part of the program consisted of detailed pressure measurements in the wind tunnel on a harmonically oscillating wing/tip tank/store configuration. Recently results of this experimental investigation were presented by Renirie.[1] The second part involved the development of a method for the calculation of aerodynamic loads on oscillating wing/body combinations in subsonic flow. Since the latter method should provide data for aeroelastic analysis as well as data to support wind tunnel measurements, it was required that both local and overall aerodynamic coefficients and generalized aerodynamic coefficients, as well as detailed pressure distributions on the wing and on the bodies, could be calculated.

Until recently the loading introduced by the bodies was either neglected completely or approximated using slender-body theory only. An early attempt to calculate more thoroughly wing/body interference effects on oscillating configurations was made by Kalman, Rodden, and Giesing.[2] In an application of the doublet-lattice method they were able to give a reasonable prediction of the interference effects on the wing due to the proximity of the body. However, their ring-wing approximation of the body prohibited a meaningful calculation of forces on the body itself. Later, to overcome this restriction, they introduced a slender body formulation

Presented as Paper 75-864 at the AIAA 8th Fluid and Plasma Dynamics Conference, Hartford, Conn., June 16-18, 1975; submitted July 14, 1975; revision received Dec. 7, 1976.

Index categories: Aerodynamics; Nonsteady Aerodynamics; Aeroelasticity and Hydroelasticity.

*Senior Research Engineer, Dept. of Aeroelasticity. Member AIAA.

†Research Engineer, Dept. of Applied Mathematics.

‡Senior Research Engineer, Dept. of Aeroelasticity.

into their method.[3] And finally, to keep the system of equations within reasonable bounds, they incorporated an image system to take care of the interference effects.[4] The method thus obtained gives quite satisfactory results as far as the calculation of aerodynamic coefficients is concerned.

Lately, Morino[5] described a calculation method for steady as well as unsteady subsonic and supersonic flow about complex configurations, applying source and dipole distributions. This method can provide pressure distributions, aerodynamic coefficients, and generalized aerodynamic coefficients for harmonically oscillating configurations. Such results have been presented in Ref. 6. For isolated and interfering lifting surfaces the agreement with experiment and lifting surface theory is good. However, for a wing/body/tail configuration, the lack of comparative results prevents a conclusion about the successful prediction of the unsteady loading on the oscillating body and the interference toward the lifting surfaces.

The method developed at NLR (NLRI method) is set up to calculate detailed pressure distributions on bodies as well as lifting surfaces. To this end the doublet-lattice method is combined with an unsteady source panel method. To introduce the effects of the distortion of the steady flowfield due to the thickness of the body, the possibility is built in of a coupling with a steady method, which itself is a combination of a vortex-lattice method and a steady source panel method. The complete NLRI method is described in detail in Ref. 7.

In the present paper only a short outline of the calculation method will be given. Emphasis is placed on the applicability of the method, which will be demonstrated in a comparison of calculated and experimental pressure and load distributions on the aforementioned oscillating wing/tip tank/pylon/store configuration.

Outline of the Calculation Method

When describing the airloads on a wing/body configuration the elements of such a configuration can be divided into two parts: relatively thin lifting surfaces (wing, pylon, fin, and stabilizer), and more or less streamlined closed bodies (fuselage, pylon-stores, and wingtip tank). Each of these elements influences the others through interference effects.

In the setup of the present calculation method the distinction between the two types of elements was used explicitly. The unsteady aerodynamic forces on the lifting surfaces are calculated with the doublet-lattice method. In this method the thickness of the lifting surfaces is neglected and only the effect of the dynamic angle of attack is taken into account. This method has been chosen for two reasons. First, comparisons of a large number of calculated and experimental results have shown that in general the neglect of wing thickness has not hampered a satisfactory agreement. Secondly, as shown in Refs. 2, 3, 8, and 9, by applications to widely different lifting surface configurations, the doublet-lattice method in particular has proved to be very flexible in handling different configurations of interfering surfaces (including the simulation of an engine nacelle).

An unsteady source panel method has been chosen to describe the flowfield about the bodies, of which the thickness is not neglected. This choice has been made, first because detailed pressure distributions are required, and second because at NLR at lot of experience with steady source panel methods is available.[10] The interference effects between the different parts of the configuration are realized by coupling the formulations of both methods through the boundary conditions imposed on all surfaces.

The flowfield about the oscillating configuration is described with the velocity potential, consisting of a freestream part and a perturbation potential φ. This perturbation potential satisfies the linearized equation

$$\beta^2\varphi_{xx}+\varphi_{yy}+\varphi_{zz}-\frac{1}{a_\infty^2}\varphi_{tt}-\frac{2M_\infty}{a_\infty}\varphi_{xt}=0 \tag{1}$$

subject to the boundary condition

$$\frac{DS}{Dt}=\frac{\partial S}{\partial t}+\boldsymbol{q}\cdot\nabla S=0 \quad (S=0) \tag{2}$$

requiring the flow to be tangential to the surface of the oscillating wing/body configuration, described by

$$S(x,y,z,t)=0 \tag{3}$$

The potential φ is divided into a steady part φ_0 and a harmonically oscillating part $\varphi_1 e^{i\omega t}$. As shown in Ref. 7, this division makes it possible for Eq. (1) to be transformed into the Laplace equation for φ_0, describing the steady flowfield, and the Helmholtz equation for φ_1, describing the unsteady flowfield. Using this, the general solution of Eq. (1) for φ_0 and φ_1 can be expressed in terms of an intergral over a steady and an unsteady source distribution on the surface of the body and the lifting surfaces, together with an integral over a steady and an unsteady dipole distribution on the camber surfaces and the wake. Since in the present method the lifting surfaces are assumed to be infinitely thin, the distributions on these parts are reduced to only a dipole distribution on the camber and wake surfaces. The strength of the distributions has to be determined by specifying the boundary conditions, of which the detailed forms for the steady and unsteady parts of the flowfield are derived in Ref. 7 under the assumption of small oscillation amplitudes. Applying these conditions leads to two sets of integral equations for the steady and the unsteady distributions. The actual expressions are given in the Appendix.

Dividing the potential in a steady and an unsteady part, as indicated previously, results in a decoupling of the steady and unsteady flowfields. However, Eq. (A9) shows that for bodies this coupling can be restored if, in the boundary condition, terms of the order of φ_0 are not neglected as compared to terms of the order of q_∞. In that case the effects of the local changes in the steady flowfield due to the presence of the bodies are introduced again in the unsteady calculation.

To solve the integral equations (A7-A9), the distributions are discretized by dividing the bodies and lifting surfaces into N_B and N_D panels, respectively. The panels on the bodies are assumed to contain a source distribution of constant yet unknown strength σ_n. The dipole distribution on each panel of the lifting surfaces is taken to be concentrated in a lifting line of strength ΔC_{p_n}, positioned along the ¼-chord line of the panel. In addition each panel possesses a collocation point in which the boundary condition is imposed. With this discretization the integral equations are reduced to two sets of (N_B+N_D) algebraic equations

$$\left[\sum_{j=1}^{N_B} A_n^{ij}\sigma_n^j+\sum_{j=1}^{N_D} A_n^{ij}\Delta C_{p_n}^j=F_n^i\right]_{i=1,2,\ldots(N_B+N_D)} \quad (n=0,1) \tag{4}$$

The term F_n^i is the prescribed normal velocity in the collocation point of the ith panel of either the body or the lifting surface. The influence coefficient A_n^{ij} represents the normal velocity induced by the jth panel with a source distribution or lifting line of unit strength in the collocation point of the ith panel. Their method of calculation as well as the numerical procedure to solve Eq. (4) are given in the next section.

After the source and lifting line strength have been calculated, the pressure distributions can be determined. For the lifting surfaces the strength of the lifting lines is taken to be equal to the pressure jump over the surface in the middle of the ¼-chord line of the panel. The steady and unsteady pressure distributions on the bodies follow from the expressions given in the Appendix. Equation (A12) for the unsteady pressure distribution on the bodies shows a similar coupling with the steady flowfield as is explained for the integral equation (A9).

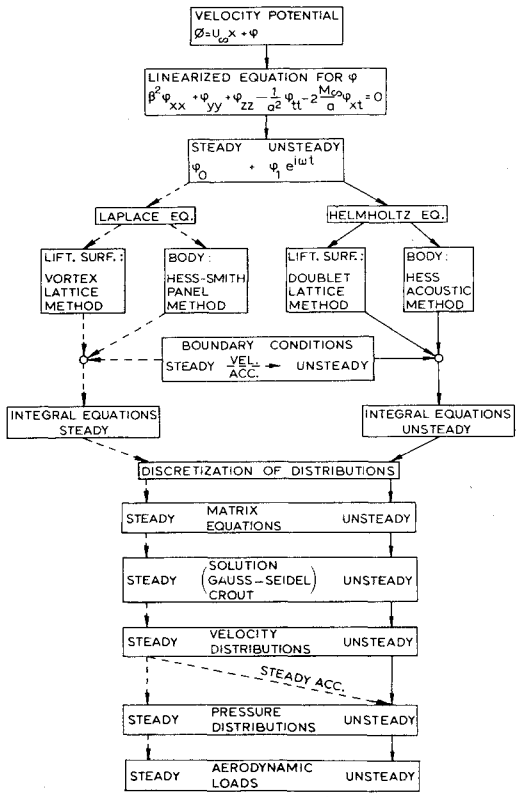

Fig. 1 Schematic outline of the calculations.

A schematic diagram of all necessary calculations is given in Fig. 1.

Numerical Calculations

For the steady flowfield, the calculation of the influence coefficients A_0^{iB} and A_0^{iD} is made with the expressions of the source panel method of Hess and Smith[11] and the vortex-lattice method, respectively. Accordingly, the doublet-lattice method is used for the unsteady coefficients A_l^{iD}.

A new calculation procedure has been developed to evaluate the unsteady coefficients A_l^{iB}, expressed by the integral

$$A_l^{iB}\langle x,y,z\rangle = -\frac{1}{4\pi}\iint_{S_B}\left[\nabla\left(e^{ik_l M_\infty(x-\xi_B)}\frac{e^{-ik_l r}}{r}\right)\right]\cdot n\langle x,y,z\rangle \mathrm{d}S \quad (5)$$

This procedure is partly based on formulations given by Hess[12] for his acoustic panel method for arbitrarily shaped bodies. The method by which the integral is evaluated depends on the ratio r_c/t, the distance between collocation point i and the centroid of the panel j on the body over the longest diagonal of this panel. The following regions are distinguished:

1) $r_c/t \geq 4$: the point i lies far away from panel j; the source distribution on the panel is approximated with a point-source at the centroid of the panel.

2) $4 > r_c/t \geq 1.9$: the point i lies at fairly large distance from panel j; the source distribution is approximated with a two-term multipole expansion in powers of $(k_l t)$ and (t/r_c) around the centroid.

3) $1.9 > r_c/t \geq 1$: the point i lies at fairly small distance from panel j; the same approximation as in 2), with three terms taken into account instead of two.

4) $1 > r_c/t > 0$: the point i lies close to the centroid of panel j; the integrand is approximated with a one-dimensional Taylor series expansion in powers of $(ik_l r)$.

5) $r_c/t = 0$: the point i lies at the centroid of panel j; the integrand is expanded similarly as in 4), but now the expressions are simpler.

A detailed description of the above approximations and the resulting expressions are given in Ref. 13.

Making a distinction between bodies and lifting surfaces, the set of algebraic equations (4) can be written in matrix form as follows

$$\begin{bmatrix} A_n^{BB} & A_n^{BD} \\ A_n^{DB} & A_n^{DD} \end{bmatrix}\begin{bmatrix} \sigma_n \\ \Delta C_{p_n} \end{bmatrix} = \begin{bmatrix} F_n^B \\ F_n^D \end{bmatrix} \quad (n=0,l) \quad (6)$$

in which the matrix is partitioned into four submatrices, each containing the coefficients of a particular type of influence between panels on the bodies and/or the lifting surfaces. The advantage of this partitioning is that the method of solution can be based on the expected properties of the submatrices. This has led to the following procedure: First the subset of equations containing $[A_n^{BB}]$ is solved with an iterative Gauss-Seidel process. Then the residue is determined and used to solve the set containing $[A_n^{DD}]$ with a direct Crout process. The residue is determined again and the process is started from the beginning. This iteration process is repeated several times until the increment, which during each run is added to the solution of σ_n and ΔC_{p_n}, has become smaller than a certain value. A relaxation factor takes care of large oscillations during the first few iteration steps.

In the calculations of the examples to be discussed in the next section the coupling between the steady and unsteady flowfield has not been made. As can be seen in Eqs. (A9) and (A12), the realization of this coupling requires the evaluation of the second derivatives of φ_0. But the values obtained in preliminary calculations with the steady version of the method were not everywhere small, i.e., of the same order as φ_0 and $\nabla\varphi_0$. Instead, locally at places with a relatively small radius of curvature they were so large that they dominated the solution completely. Reducing the size of the panels did not yield a significant improvement. Apparently the concept of small disturbances, on which this unsteady method is based, is violated as far as the second derivatives of φ_0 are concerned. Since they appear only locally one can argue that their influence on the unsteady pressure distributions will be of minor importance. This might explain the still satisfactory agreement with experimental data, obtained while neglecting the coupling.

Comparison of Calculated and Experimental Results

To verify the theory and to show the applicability of the method, several calculations have been made for the model tested in the wind tunnel as a part of the NLR wing/store program previously mentioned. This model, shown in Fig. 2, consists of a tapered wing with a wingtip tank and a removable pylon/store combination. Measured results where obtained for pitching oscillations around an axis at 15% of the root chord. The calculations and comparison with experimental data are made at $M_\infty = 0.45$ and a reduced frequency $k = 0.305$ (based on the semispan) for two configurations: 1) wing with tip tank only, and 2) wing with tip tank, pylon, and store.

Panel Distributions

Before describing the panel distributions used for the aforementioned configurations, some observations should be made about the panelling near the intersection of a lifting surface and a body. It is clear that if the panelled lifting surface would terminate at the body surface, large normal

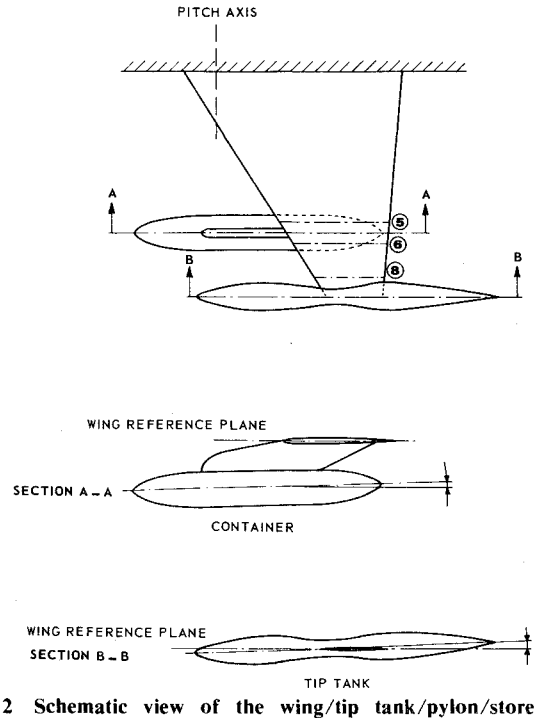

Fig. 2 Schematic view of the wing/tip tank/pylon/store configuration.

velocities would be induced on this body surface. This would result in considerable errors in the calculated pressures near the junction. The usual way to overcome this is the use of an image system, obtained by mapping the singularities on the wing to the inside of the body (see Ref. 4). This method works very well if the body can be represented by an infinitely long cylinder. However, in the case of a closed body, the accuracy can become problematic near the panels where the trailing vortices of the image system intersect through the rear of the body.

For the present calculations a simplified approximate image system is used, in which the lifting surface is assumed to continue toward the centerline of the body. The part inside the body is covered with one strip of panels. The strength of the lifting lines is taken to be equal to the adjacent strip outside the body and thus no additional collocation points are required. The reasons for using this simple type of image system are as follows:

1) Numerical problems near the attachment line of the lifting surface and the body are avoided.

2) Application of this system in the NLR steady panel method[10] has given good results.

3) For symmetric flow conditions around a fuselage, the centerline trailing vortex is absent.

4) The wake of the body is not neglected, since it is represented by the wake of the extension of the lifting surface into the body. The number of trailing vortices intersecting the rear of the body is reduced to one.

Table 1 Panel distributions

	Chordwise		Spanwise		Total	Inside body
Wing	10	×	9	=	90	10
Pylon	10	×	2	=	20	10
Lifting surfaces					110	
	Direction					
	Axial		Angular		Total	
Wingtip tank	27	×	8	=	216	
Store	19	×	8	=	152	
Bodies					368	

The panel distribution as used in the present calculations is shown in Table 1. The wingtip tank and the store are divided into 27 and 19 sections, respectively. Each circular section, being perpendicular to the body axis, contains eight quadrilateral panels, of which the corner points are positioned on the body surface. The wing is covered with ten chordwise strips of ten panels each. The outwardmost strip is assumed to continue within the tip tank to the tip tank axis in such a way that parts of these panels are located within the tip tank. The pylon contains three chordwise strips of ten panels each. Here the lowest strip is placed in the upper half of the container ending at the container axis.

Wing/Tip Tank Configuration

Figure 3 shows the chordwise distribution of the unsteady pressure jump ΔC_{p_l} across the wing in a section close to the tip tank. The effect induced by the tip tank on the wing is evident by comparing the theoretical distributions with and without tip tank, the latter being obtained with the doublet-lattice method only. Adding the tip tank results in an increase of ΔC_{p_l}. Considering the agreement between the calculated and experimental results, this interference effect is predicted rather well. The unsteady spanwise load distribution on the wing is given in Fig. 4. The theoretical curves indicate that for the wing the tip tank acts as a type of endplate. With the tip tank attached, the load distribution remains at a higher level and does not reach zero at the tip. Clearly, the interference effects are largest in the vicinity of the tip. The agreement between the calculated and experimental results is reasonable, showing the same trend. The differences are of the same order as found in earlier comparisons for lifting surfaces only.[8]

In Fig. 5 an example is given of an unsteady pressure distribution in the axial direction along the tip tank. Except for the rear part, where in reality the flow is separated, the

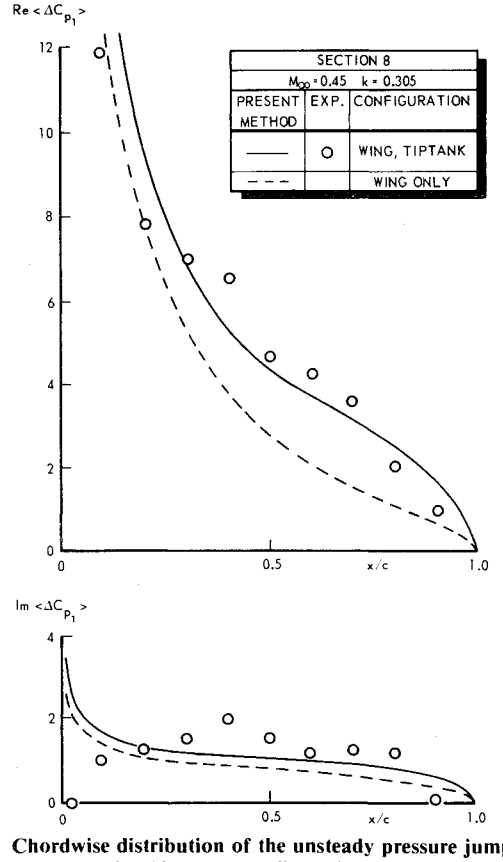

Fig. 3 Chordwise distribution of the unsteady pressure jump across the wing of the wing/tip tank configuration oscillating in a pitch mode.

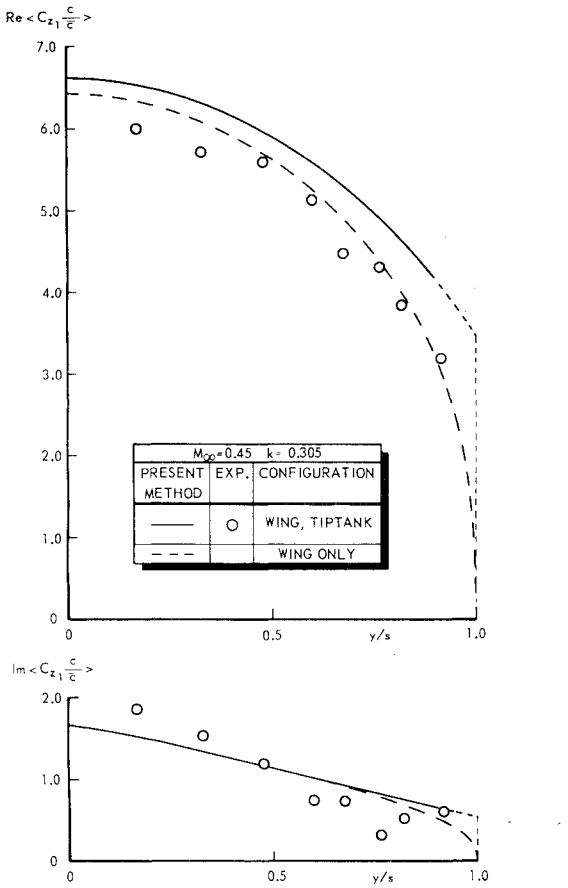

Fig. 4 Unsteady normal load distribution on the wing of the wing/tip tank configuration oscillating in a pitch mode.

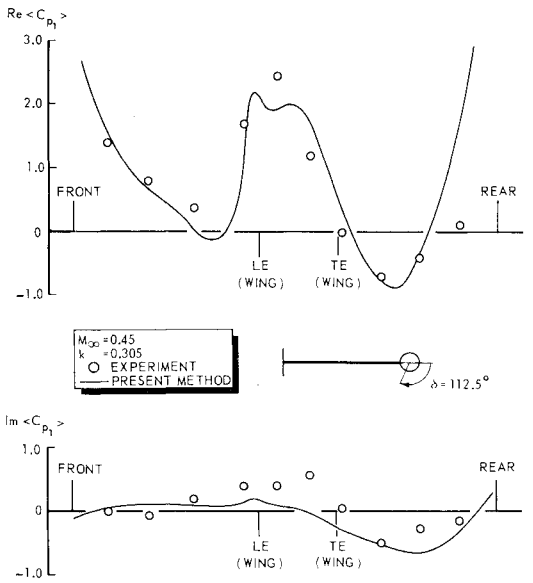

Fig. 5 Unsteady pressure distribution along the tip tank of the wing/tip tank configuration oscillating in a pitch mode.

agreement is rather good. The differences between theory and experiment are of the same order as they are on the wing. The theoretical curve shows the influence of the wing in the relatively large positive pressures near the attachment position. The peak at the wing leading edge is too small to be discernable in the measurements. The corresponding normal load distribution obtained by integration in the angular direction is shown in Fig. 6. Here the calculated curves go to zero at the front and rear ends yielding a better agreement with measured values. In comparing the normal load

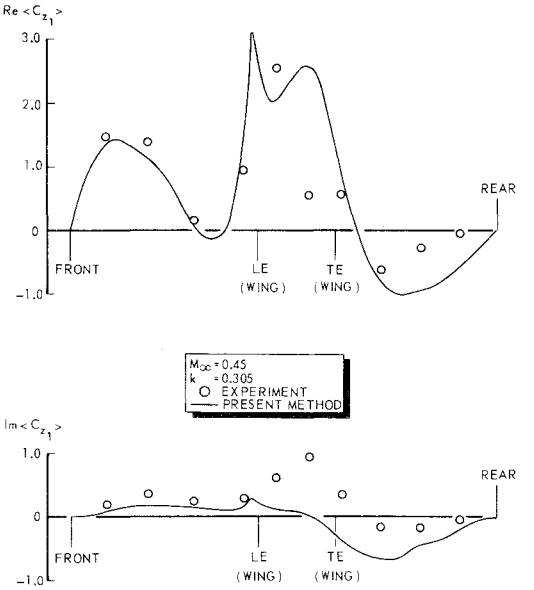

Fig. 6 Unsteady normal load distribution along the tip tank of the wing/tip tank configuration oscillating in a pitch mode.

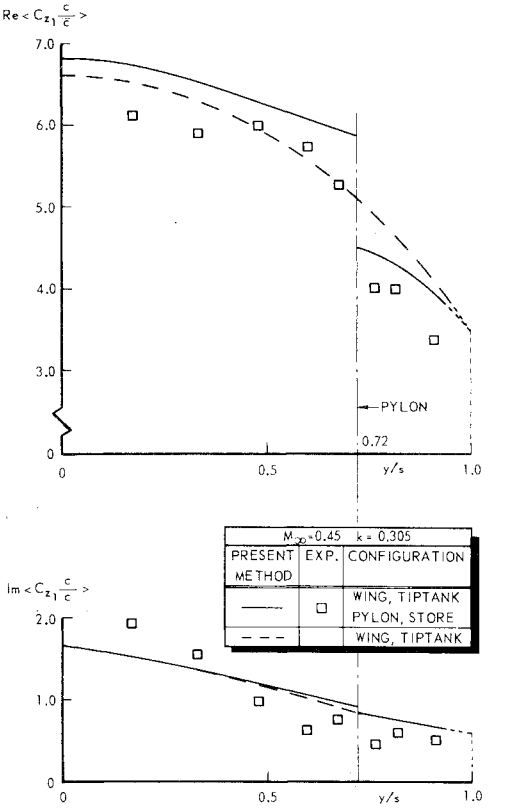

Fig. 7 Normal load distribution on the wing of the wing/tip tank/pylon/store configuration oscillating in a pitch mode.

distributions on the tip tank and the wing, it should be realized that both are nondimensionalized in a different way. To make them comparable the tip tank value should be multiplied by the factor 0.2 (max. diam/$\bar{c}$). In doing so it follows from Figs. 4 and 6 that the load on the tip tank is of the order of 0.1 of the wing loading. Note that especially the imaginary part is extremely small.

Wing/Tip Tank/Pylon/Store Configuration

Adding the pylon and store to the configuration introduced a jump in the spanwise load distribution at the place of the

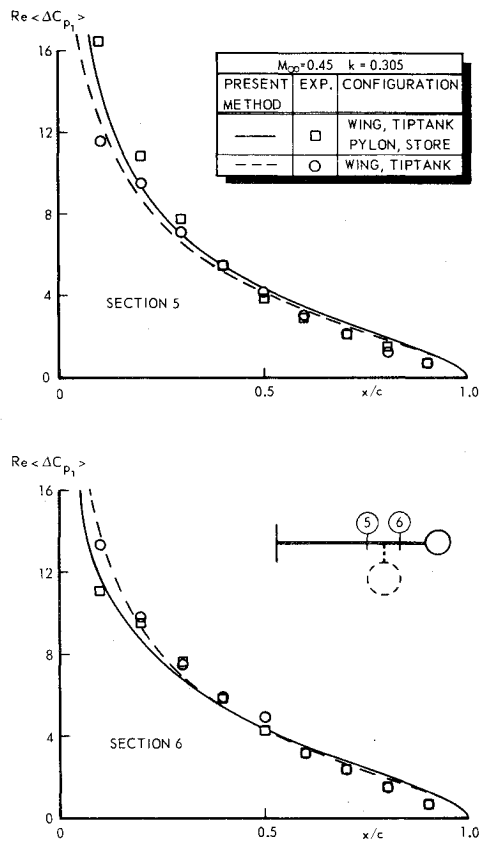

Fig. 8 The effect of the addition of the pylon and store on the chordwise distributions of the real part of the unsteady pressure jump across the wing on both sides of the pylon.

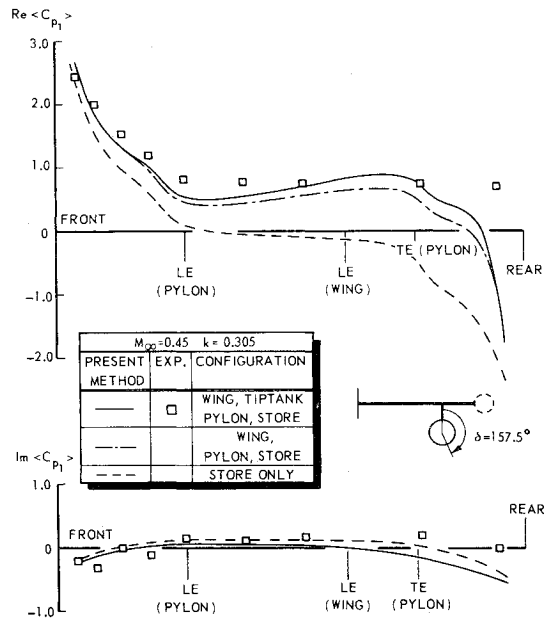

Fig. 9 Unsteady pressure distribution along the store of the wing/tip tank/pylon/store configuration oscillating in a pitch mode.

pylon attachment, of which the real part is by far the largest one. This is shown in Fig. 7 where the calculated distributions are given for the configurations both with and without the pylon and store. The experimental results show a jump of about the same magnitude, although, as in Fig. 4, the overall level is slightly different. This jump in both the theoretical and experimental curves can be explained in terms of the chordwise pressure distribution on either side of the pylon. Figure 8 shows that the addition of the pylon and store affects

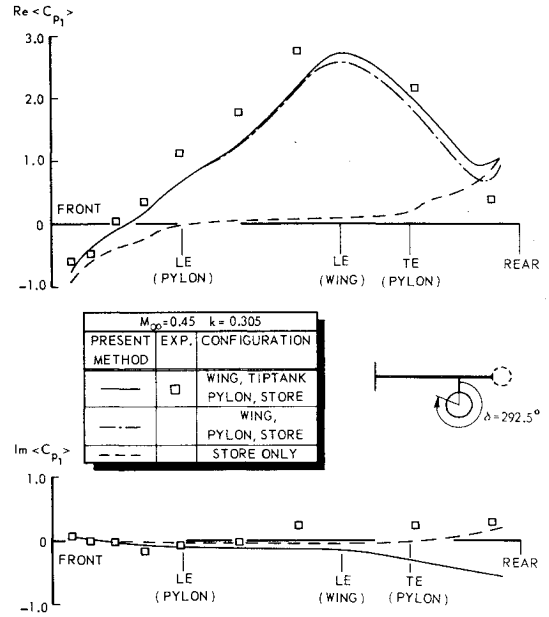

Fig. 10 Unsteady pressure distribution along the store of the wing/tip tank/pylon/store configuration oscillating in a pitch mode.

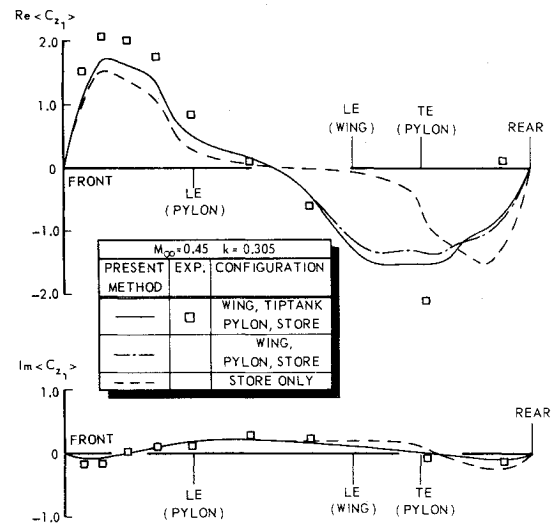

Fig. 11 Unsteady normal load distribution along the store of the wing/tip tank/pylon/store configuration oscillating in a pitch mode.

mainly the pressure peaks near the leading edge of the wing. Inboard of the pylon this peak increases, while outboard a decrease is observed. As a jump in the normal load distribution indicates a jump in the circulation around the wing, obviously circulation is carried off by the pylon. As a result of this the pylon will experience an outward pointing load.

Figures 9 and 10 give the unsteady pressure distribution along the store at two angular positions. Both figures show calculated pressure distributions for three types of configurations: the store alone, and the wing/pylon/store combination with and without tip tank. Comparing these distributions, it is clear the addition of the wing and pylon has a marked effect. On the store this interference effect is largest near the attachment of the pylon and store, with a maximum in the vicinity of the leading edge of the wing where the flowfield is disturbed most. Adding the tip tank gives a slight increase of the real part of the pressure distribution over the rear section of the store, while the imaginary part is not visibly affected. The explanation can be found in Fig. 4, where it is shown that the addition of the tip tank increases the normal load distribution and thus the circulation around the

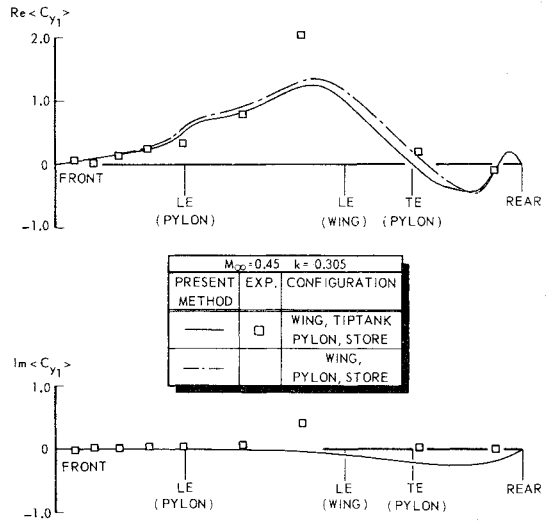

Fig. 12 Unsteady side load distribution along the store of the wing/tip tank/pylon/store configuration oscillating in a pitch mode.

wing. The resulting change in the velocity field under the wing is the cause of the increased pressures on the store.

The agreement between the calculated and the experimental pressure distributions is reasonably good. It is felt by the authors that the agreement could be even better if in the panelling process the corner points are not put on the surface of the store, but slightly outside. With the eight panels used in angular direction this will effectively bring the cross-sectional area of the panelled store back to that of the original store.

The normal and side load distributions on the store are given in Figs. 11 and 12. On the isolated store the normal load distribution is symmetrical, with a sign change in the real part. This is not surprising since the store has identical front and rear ends connected by a cylindrical part. On this cylindrical midsection the load is very small, which is also characteristic for slender-body theory. The results of Fig. 11 clearly show the large interference effects from the wing and pylon on the normal load distribution. The side load on this rotationally symmetric store (see Fig. 12) would be nonexistent without these interference effects. The direction of the side load on the store coincides with the direction of the load on the pylon as inferred from the jump in the circulation around the wing. The addition of the tip tank has only a small influence on both load distributions, while the experimental values are predicted rather well. As in the case of the tip tank, a comparison between the loading on the wing and the store is only possible if the values for the store are multiplied by a factor of 0.26 (max. diam/$\bar{c}$). This means that the loading on the store is about 7% of the wing loading and that the imaginary part is negligibly small.

Concluding Remarks

A method has been presented which enables the calculation of unsteady pressure distributions on wing/body configurations in subsonic flow. The applicability of the method has been shown in a comparison with experimental results for a wing/tip tank/pylon/store configuration. Both pressure and load distributions on the wing and the bodies are in reasonable agreement with the measurements. The interference effects are predicted very well.

The loading on the tip tank and the store has been found to be of the order of 10% of the wing loading. The imaginary part of the loads on these bodies is negligibly small. This might indicate that in aeroelastic calculations not much damping can be expected from these aerodynamic forces in specific store modes.

The coupling between the steady flowfield and the superimposed unsteady flowfield, which can be taken into account in the present method, could not be realized successfully. However, the agreement between theoretical and experimental data, shown here, is such that no immediate need exists to improve the evaluation of this influence in the present case.

In view of applications in flutter calculations when unsteady aerodynamic forces are needed for a large number of Mach numbers, reduced frequencies, and store configurations, it is worthwhile to investigate whether or not body influence has to be considered or simplifications are possible, i.e., to represent a store by an endplate. The present method then can provide useful data for comparison. Another field of application may be the calculation of dynamic stability derivatives, especially those in which a considerable contribution of the fuselage is involved.

Appendix

Reference 9 shows that, for a configuration of bodies and infinitely thin lifting surfaces harmonically oscillating in subsonic flow, the general solution of Eq. (1) can be formulated as

$$\varphi\langle x,y,z,t\rangle = \varphi_0\langle x,y,z\rangle + \varphi_1\langle x,y,z\rangle e^{i\omega t} \tag{A1}$$

where, for the body

$$\varphi_n^B\langle x,y,z\rangle = -\frac{1}{4\pi}\iint_{S_B} \sigma_n\langle \xi_B,\eta_B,\zeta_B\rangle e^{ik_n M_\infty (x-\xi_B)} \frac{e^{-ik_n r}}{r}\,dS \tag{A2}$$

in which

$$r=[(x-\xi_B)^2+\beta^2(y-\eta_B)^2+\beta^2(z-\zeta_B)^2]^{1/2} \tag{A3}$$

and for the lifting surface

$$\varphi_n^D\langle x,y,z\rangle = \frac{q^2}{8\pi U_\infty}\iint_{S_D} \Delta C_{p_n}\langle \xi_D,\eta_D,\zeta_D\rangle K_n\langle x,y,z,\xi_D,\eta_D,\zeta_D,M_\infty,\omega\rangle dS \tag{A4}$$

in which

$$K_n = e^{-in\omega(x-\xi_D)/U_\infty}\int_{-\infty}^{x-\xi_D}\frac{\partial}{\partial n}\left[\frac{e^{-in\omega(\tau-M_\infty r)/U_\infty\beta^2}}{r}\right]d\tau \tag{A5}$$

and

$$r=[\tau^2+\beta^2(y-\eta_D)^2+\beta^2(z-\zeta_D)^2]^{1/2} \tag{A6}$$

In the above expressions σ_n represents the strength of the source distribution on the body surfaces S_B, and ΔC_{p_n} is the strength of the dipole distribution on the lifting surfaces S_D. The subscript n can have the values 0 and 1, indicating the steady and unsteady potential.

Substitution of the above expressions in the boundary conditions derived in Ref. 9 leads to the following set of integral equations for the steady flowfield

$$-\frac{1}{4\pi}\iint_{S_B}\sigma_0\langle\xi_B,\eta_B,\zeta_B\rangle\left[\nabla\frac{1}{r}\right]_B\cdot n_B dS + \frac{q^2}{8\pi U_\infty}\iint_{S_D}\Delta C_{p_0}\langle\xi_D,\eta_D,\zeta_D\rangle[\nabla K_0]_B\cdot n_B dS = -q_\infty\cdot n_B \tag{A7}$$

$$-\frac{1}{4\pi}\iint_{S_B}\sigma_0\langle\xi_B,\eta_B,\zeta_B\rangle\left[\nabla\frac{1}{r}\right]_D\cdot n_D dS + \frac{q_\infty^2}{8\pi U_\infty}\iint_{S_D}\Delta C_{p_0}\langle\xi_D,\eta_D,\zeta_D\rangle[\nabla K_0]_D\cdot n_D dS = -q_\infty\cdot n_D \tag{A8}$$

and for the unsteady flowfield

$$-\frac{1}{4\pi}\iint_{S_B}\sigma_1\langle\xi_B,\eta_B,\zeta_B\rangle\left[\nabla\left(e^{ik_1M_\infty(x-\xi_B)}\frac{e^{-ik_1r}}{r}\right)\right]_B\cdot\boldsymbol{n}_B\mathrm{d}S$$

$$+\frac{q_\infty^2}{8\pi U_\infty}\iint_{S_D}\Delta C_{p_1}\langle\xi_D,\eta_D,\zeta_D\rangle[\nabla K_1]_B\cdot\boldsymbol{n}_B\mathrm{d}S$$

$$=-i\omega\boldsymbol{r}_e^*\cdot\boldsymbol{n}_B+(q_\infty+\nabla\varphi_0)\cdot(\ell_B\nabla_0\ x_e^*+m_B\nabla_0\ y^*+n_B\nabla_0\ z_e^*)$$

$$+\boldsymbol{n}_B[(\boldsymbol{r}_e^*\cdot\nabla)\nabla\varphi_0]_B \qquad \text{(A9)}$$

$$-\frac{1}{4\pi}\iint_{S_B}\sigma_1\langle\xi_B,\eta_B,\zeta_B\rangle\left[\nabla\left(e^{ik_1M\ (x-\xi_B)}\frac{e^{-ik_1r}}{r}\right)\right]_D\cdot\boldsymbol{n}_D\mathrm{d}S$$

$$+\frac{q_\infty^2}{8\pi U_\infty}\iint_{S_D}\Delta C_{p_1}\langle\xi_D,\eta_D,\zeta_D\rangle[\nabla K_1]_D\cdot\boldsymbol{n}_D\mathrm{d}S$$

$$=i\omega\boldsymbol{r}_e^*\cdot\boldsymbol{n}_D+q_\infty\cdot(m_D\nabla_0 y_e^*+n_D\nabla_0 z_e^*) \qquad \text{(A10)}$$

Equations (A7) and (A8) determine the steady flowfield about the bodies and the lifting surfaces, while Eqs. (A9) and (A10) concern the unsteady flowfield superimposed on this steady field. The interference effects between the bodies and the lifting surfaces are represented in the second integral of Eqs. (A7) and (A9) and in the first integral of Eqs. (A8) and (A10).

After the steady source and lifting line strength have been calculated, the first and second derivatives of φ_0 also can be determined analytically. Next, these values are used to determine the right-hand side of the unsteady set of equations, after which the unsteady flowfield can be solved for as well.

For the lifting surfaces the strength of the lifting line is taken to be equal to the pressure jump over the surface. The steady and unsteady pressure distributions on the bodies follow from the following expressions, derived in Ref. 9

$$C_{p_0}=\frac{2}{\gamma M_\infty^2}\left\{\left[1+\frac{(\gamma-1)}{2}M_\infty^2\left(1-\frac{\boldsymbol{q}_0\cdot\boldsymbol{q}_0}{q_\infty^2}\right)\right]^{\gamma/(\gamma-1)}-1\right\} \qquad \text{(A11)}$$

and

$$C_{p_1}=-\frac{2}{q_\infty^2}\left[1-\frac{(\gamma-1)}{2}M_\infty^2\left(1-\frac{\boldsymbol{q}_0\cdot\boldsymbol{q}_0}{q_\infty^2}\right)\right]^{1/(\gamma-1)}$$

$$\times[\boldsymbol{q}_0\cdot\nabla\varphi_1+i\omega\varphi_1+(U_\infty+\varphi_{0_x})(\boldsymbol{r}_e^*\cdot\nabla)\varphi_{0_x}$$

$$+(V_\infty+\varphi_{0_y})(\boldsymbol{r}_e^*\cdot\nabla)\varphi_{0_y}+(W_\infty+\varphi_{0_z})(\boldsymbol{r}_e^*\cdot\nabla)\varphi_{0_z}] \qquad \text{(A12)}$$

in which

$$\boldsymbol{q}_0=(U_\infty+\varphi_{0_x})\boldsymbol{i}+(V_\infty+\varphi_{0_y})\boldsymbol{j}+(W_\infty+\varphi_{0_z})\boldsymbol{k} \qquad \text{(A13)}$$

Acknowledgment

This paper summarizes work carried out under contract for the Scientific Research Branch, Air Material Directorate, Royal Netherlands Air Force.

References

[1] Renirie, L.T., "Analysis of Measured Aerodynamic Loads on an Oscillating Wing/Store Combination in Subsonic Flow," *AGARD Specialists Meeting on Wing-with-Stores Flutter,* CP-162, Paper No. 5, Munich, 1974.

[2] Kalman, T.P., Rodden, W.P., and Giesing, J.P., "Application of the Doublet-Lattice Method to Nonplanar Configurations in Subsonic Flow," *urnal of Aircraft,* Vol. 8, June 1971, pp. 406-413.

[3] Rodden, W.P., Giesing, J.P., and Kalman, T.P., " New Developments and Applications of the Subsonic Doublet Lattice Method for Nonplanar Configurations," *AGARD Conference Proceedings,* CP-80-71, Part II, No. 4, 1971.

[4] Giesing, J.P., Kalman, T.P., and Rodden, W.P., "Subsonic Steady and Oscillatory Aerodynamics for Multiple Interfering Wings and Bodies," *Journal of Aircraft,* Vol. 9, Oct. 1972, pp. 693-702.

[5] Morino, L.,"A General Theory of Unsteady Compressible Potential Aerodynamics," CR-2464, Dec. 1974, NASA.

[6] Tseng, K. and Morino, L., "Fully Unsteady Subsonic and Supersonic Potential Aerodynamics of Complex Aircraft Configurations for Flutter Applications," *Proceedings of the AIAA/ASME/SAE 17th Structures, Structural Dynamics and Materials Conference,* King of Prussia, Pa., May 1976, pp. 626-638.

[7] Bennekers, B., Roos, R., and Zwaan, R.J., "Calcon of Aerodynamic Loads on Oscillating Wing/Store Combinations in Subsonic Flow," *AGARD Specialists Meeting on Wing-with-Stores Flutter,* CP-162, Paper No. 4, Munich, 1974.

[8] Roos, R. and Zwaan , R.J., "Calculation of Instationary Pressure Distributions and Generalized Aerodynamic Forces with the Doublet-Lattice Method," NLR TR 72037 U, 1972, National Aerospace Laboratory NLR, Amsterdam.

[9] Roos, R. and Zwaan, R.J., "The Effect of a Pylon-Mounted Nacelle on the Flutter Behaviour of a Wing-Pylon-Nacelle figuration," NLR TR 74125 U, 1974, National Aerospace Laboratory NLR, Amsterdam.

[10] Labrujere, Th.E. and Sytsma, H.A., "Aerodynamic Interference between Aircraft Components: The Possibility of Predication," *Proceedings of the 8th Congress of the International Council of Aeronautical Sciences,* Paper No. 72-49, Amsterdam, August 1972.

[11] Hess, J.L. and Smith, A.M.O., "Calculation of Potential Flow about Arbitrary Bodies," *Progress in Aeronautical Sciences,* Vol. 8, Kuchemann, D., ed., Pergamon, London, 1967, pp. 1-138.

[12] Hess, J.L., "Calculation of Acoustic Fields about Arbitary Three-Dimensional Bodies by a Method of Surface Source Distributions Based on Certain Wave Number Expansions," Douglas Aircraft Company, Long Beach, Calif., DAC 66901, March 1968.

[13] Roos, R., and Bennekers, B., "Description of a Method for the Calculation of Aerodynamic Loads on Oscillating Wing-Body Configurations," National Aerospace Laboratory NLR, Amsterdam, NLR TR 75044 L, 1975 (in Dutch).